Journal of the Brazilian Society of Mechanical Sciences and Engineering (2021) 43:196
https://doi.org/10.1007/s40430-021-02889-7

TECHNICAL PAPER

Numerical study of the wave dissipation performance of two plate-type open breakwaters based on the Navier–Stokes equations

Xueyan Li[1,2] · Tian Xie[1] · Qing Wang[1] · Zhichen Zhang[1] · Chengyi Hou[1] · Weijun Guo[3] · Xiang Wan[1] · Xiaomin Xie[1]

Received: 21 May 2020 / Accepted: 9 February 2021 / Published online: 10 March 2021

Abstract
In this study, wave generation is simulated using the velocity wave generation method. A damping wave dissipation region is established to eliminate wave reflection at the flume tail. Fluid motion is described using the Navier–Stokes equations. The water free surface is captured using the volume of fluid method. A 2D numerical model for the interactions between waves and plate-type open breakwaters is constructed using the finite volume method, and their correctness is validated by experimental results. Based on these models, two plate-type open breakwaters are compared in terms of the wave transmission coefficient (K_t), wave reflection coefficient (K_r), wave energy dissipation coefficient (K_d) and wave energy distribution. By comprehensively considering K_t, K_r, K_d and the wave energy distribution, the double-arc plate-type open breakwater is found to exhibit higher wave dissipation performance.

Keywords *N–S* equations · Plate-type open breakwater · Wave dissipation performance · VOF method · Finite volume method

1 Introduction

Plate-type open breakwaters are a new type of protective structure. These breakwaters have plate-type structures and are placed near the water surface to disrupt the motion of water particles with the aim to dissipate waves based on the principle that wave energy is concentrated at the water surface. The lower section of plate-type open breakwaters is unobstructed to allow the free water flow and thus does not affect the coastal water quality and the marine ecological environment. Additionally, plate-type open breakwaters have a simple structure and are low in cost, easily constructed and relatively insignificantly affected by the water depth and geological conditions; as a result, they have recently become a focus of experts and researchers in the ocean engineering field.

Research on plate-type open breakwaters dates to the 1940s. In 1947, Ursell [1] pioneered studies on vertical plate-type open breakwaters in deep water conditions. Later, other researchers extensively studied various open breakwaters, including vertical plate-type (Koley et al. [2]; Somervell et al. [3]) and single flat plate-type (SFPT) (Hsu and Wu. [4]; Liu et al. [5, 6]; Rao et al. [7]; Liu and Li. [8]; Cho and Kim. [9]; Wu et al. [10]; Metallinos et al. [11]) breakwaters. Because of the unsatisfactory performance of SFPT open breakwaters in waters with a relatively large tidal range, T-shaped plate-type (Neelamani and Rajendran. [12, 13]; Neelamani and Gayathri. [14]; Zhan et al. [15]), double flat plate-type (DFPT) and multiple flat plate-type (Usha and Gayathri. [16]; Wang et al. [17]; Li et al. [18]; Guo et al. [19]; Cho et al. [20]; Zhang et al. [21]; Liu and Li. [22]; Fang et al. [23]) breakwaters were systematically studied to adapt to a larger tidal range. The wave dissipation effect of these breakwaters is not ideal under the action of long waves. Thus, scholars have attempted to develop other types of breakwaters, among which one of the most representative

Technical Editor: Erick Franklin.

✉ Xueyan Li
yanzi03@126.com

✉ Qing Wang
schingwang@126.com

1 Coast Institute and Institute of Sea-Crossing Engineering, Ludong University, Yantai 264025, China

2 Key Laboratory of Coastal Disasters and Defence of Ministry of Education, Hohai University, Nanjing 210098, China

3 College of Environmental Sciences and Engineering, Dalian Maritime University, Dalian 116026, China

is the arc plate-type (APT) breakwater (Wang et al. [24]; Li et al. [25]).

An APT open breakwater is a new open breakwater structure consisting of a single or multiple arc-shaped plates. This type of breakwater was proposed by Wang et al. [26] based on semicircular breakwaters and flat plate-type (FPT) open breakwaters. Wang et al. [26] systematically investigated the effects of the plate spacing, number of plates, relative submerged depth, relative wave height and relative plate width on wave dissipation based on physical model experiments. They compared the results with the wave dissipation performance of an FPT open breakwater under the same conditions and found that the APT open breakwater exhibited higher wave dissipation performance. Wang et al. [24] analyzed the wave dissipation performance of plate-type open breakwaters using potential flow theory and found that when $D/H = 0.05$, the wave dissipation performance of an upper APT open breakwater was nearly 50% higher than that of an FPT open breakwater.

The results obtained from the aforementioned physical model experiments (Wang et al. [26]) and numerical simulations (Wang et al. [24]) demonstrate that APT open breakwaters exhibit excellent wave dissipation performance. Previous studies have made great contributions to the analysis of the wave dissipation performance of APT open breakwaters (Wang et al. [26]). However, physical model experiments have a very time- and labor-intensive preparation stage, have special requirements, and are complex processes with relatively high costs. The available numerical models (Wang et al. [24]) are based on frequency-domain potential flow theory and fail to describe large wave deformations, wave breaking and fluid viscosity effects and therefore differ significantly from the interactions between waves and structures in actual sea conditions.

Li et al. [27] successfully addressed the problem of interactions between waves and arc crown walls using a body-fitted grid and the finite difference method. However, this method has certain limitations for studying wave breaking. With the development of high-performance computers, viscous flow models based on the Navier–Stokes equations have been used in numerical simulations of some wave-breaking phenomena (Vermeire et al. [28]). Waves will break when acting on plate-type breakwaters (Higuera et al. [29]). Li et al. [25] used a viscous flow model to discuss the wave-dissipating performance and main influencing factors of lower APT breakwaters. In this study, considering the aforementioned problems of the available studies, numerical models for the interactions between waves and double-arc plate-type (DAPT) and DFPT open breakwaters are constructed using the finite volume method based on the Navier–Stokes equations. DFPT and DAPT open breakwaters are compared in terms of wave-dissipating performance and energy conversion distribution under the action of long waves. Based on this, an open breakwater structure with excellent wave-dissipating performance is proposed. The above research results can provide a new method and reference for further study of plate-type breakwaters.

This paper is organized as follows: Sect. 1 presents an introduction primarily to the research status and developmental trend of plate-type breakwaters. Section 2 introduces and validates a numerical model, gives the governing equations and boundary conditions for this numerical model in detail, and validates this numerical model in terms of wave generation and dissipation and the experimental results of DFPT and DAPT breakwaters. Section 3 gives the numerical model design and calculation parameters. Section 4 analyzes and discusses the numerical model calculation results. Section 5 presents some important conclusions derived from the results.

2 Numerical model

A second-order Stokes wave is generated on the left side of a numerical flume using the velocity wave generation method. A damping region is established on the right side of the numerical flume to eliminate wave reflection at the flume tail. The Navier–Stokes equations are used as governing equations to describe the wave motion. The water surface or the air–water interface is captured using the volume of fluid (VOF) method. A 2D numerical model of the interactions between the waves and plate-type open breakwaters is constructed using the finite volume method on the FLUENT software platform (Deng et al. [30]; Zheng et al. [31]).

2.1 Model building

2.1.1 Governing equations

$$\text{Continuity equation}: \quad \frac{\partial u}{\partial x} + \frac{\partial v}{\partial y} = 0 \tag{1}$$

$$\text{Momentum equation}: \quad \frac{\partial u}{\partial t} + u\frac{\partial u}{\partial x} + v\frac{\partial u}{\partial y} = g_x - \frac{1}{\rho}\frac{\partial p}{\partial x} + v\left(\frac{\partial^2 u}{\partial x^2} + \frac{\partial^2 u}{\partial y^2}\right) - \mu(x)u \tag{2}$$

$$\frac{\partial v}{\partial t} + u\frac{\partial v}{\partial x} + v\frac{\partial v}{\partial y} = g_y - \frac{1}{\rho}\frac{\partial p}{\partial y} + v\left(\frac{\partial^2 u}{\partial x^2} + \frac{\partial^2 v}{\partial y^2}\right) - \mu(x)v \tag{3}$$

where u and v are the fluid velocity components in the x and y directions, respectively; p is the fluid pressure; ρ is the fluid density; v is the fluid kinematic viscosity coefficient; g_x is the horizontal gravity acceleration component ($g_x = 0$); g_y is the vertical gravity acceleration component ($g_y = 9.81$ N/kg); and $\mu(x)$ is the wave dissipation coefficient ($\mu(x) = 0$ in the fluid region; $\mu(x)$ is a monotonically increasing function in the damping wave dissipation region).

The governing equations are discretized by the finite difference method. The temporal discretization of momentum equation is presented by the forward difference scheme. The eccentric difference scheme for linear combination of the first-order upwind scheme and the second-order center scheme is used to discretize the convective terms. Central difference scheme is adopted to discretize the viscous term. As the discrete scheme of the continuous equation is an implicit constraint condition, the pressure field and velocity field cannot be solved directly, and the pressure field and velocity field in the momentum equation must be solved together. In the VOF method, the SIMPLE algorithm is used to repeatedly iterate to adjust the pressure and velocity to obtain the final results.

2.1.2 Boundary conditions

(1) Free surface boundary condition

The location of the free surface of the fluid is traced using the VOF method (Li et al. [27]). A VOF function F is established to characterize the ratio of the VOF in a unit grid cell to the total volume of the unit grid cell. When $F=1$, the unit grid cell is filled with the fluid. When $F=0$, the unit grid cell is filled with air. When $0<F<1$, the unit grid cell is a free surface unit or contains the fluid mixed with small air bubbles. The VOF function $F(x, y, t)$ is defined for the center of the unit grid cell. F satisfies the following equation:

$$\frac{\partial F}{\partial t}+u\frac{\partial F}{\partial x}+v\frac{\partial F}{\partial y}=0 \tag{4}$$

where u and v are the fluid velocity components in the x and y directions, respectively, and t is time. The spatial and temporal discretization of the equation is presented by the central difference scheme.

(2) Wave generation boundary condition

The left side of the numerical flume is the wave generation boundary. A steady second-order Stokes wave is generated using the velocity wave generation method. The velocity field extends from the left flume end all the way up to the still water surface in the initial condition. The wave surface equation is given by

$$\eta=\frac{H}{2}\cos(-\omega t)+\frac{\pi H^2}{8\lambda}\frac{\cosh(kh)\,[2+\cosh(2kh)]}{\sinh^3(kh)}\cos(-2\omega t). \tag{5}$$

The equation for the velocity in the x direction is given by

$$u=f\left(\frac{t}{T}\right)\left\{\frac{\pi H}{T}\frac{\cosh[k(\eta+h)]}{\sinh(kh)}\cos(-\omega t)+0.75\frac{\pi^2H^2}{T\lambda}\frac{\cosh[2k(\eta+h)]}{\sinh^4(kh)}\cos(-2\omega t)\right\}. \tag{6}$$

The equation for the velocity in the y direction is given by

$$v=f\left(\frac{t}{T}\right)\left\{\frac{\pi H}{T}\frac{\sinh[k(\eta+h)]}{\sinh(kh)}\sin(-\omega t)+0.75\frac{\pi^2H^2}{T\lambda}\frac{\sinh[2k(\eta+h)]}{\sinh^4(kh)}\sin(-2\omega t)\right\} \tag{7}$$

where $f(t/T)$ is the startup coefficient, which controls the wave generation velocity so that it gradually increases to the target value within a certain period; H is the wave height; T is the period; t is the calculation time; η is the wave surface elevation; λ is the wavelength; h is the water depth; k is the wavenumber ($k=2\pi/L$); and ω is the circular wave frequency (ω=$2\pi/T$).

(3) Wave dissipation boundary condition

A wave dissipation region with width equal to twice the wavelength is established at the numerical flume tail to dissipate waves. Equations (2) and (3) are the governing equations for the wave dissipation region. Under these conditions, the wave dissipation coefficient $\mu(x)$ is a monotonically increasing function equal to 0 at the starting point of the damping region and to 1 at the endpoint of the damping region, as shown in Eq. (8):

$$\mu(x)=\frac{x-(L_f-L_a)}{L_a} \tag{8}$$

where x is the coordinate of the wave dissipation site; L_f is the flume length; and L_a is the wave dissipation region length.

(4) Bottom boundary condition

The bottom boundary of the numerical flume adopts the no-slip condition, and the normal velocity is 0.

2.1.3 Grid independence

To derive an optimal grid resolution, this study uses four different resolutions: very coarse, coarse, normal and fine (Table 1). N_H is the number of cells per wave height, N_L is the number of cells per wavelength, and N is the total number of cells in the computation domain. (See Table 1 for details.)

As shown in Fig. 1, the wave heights produced by the "normal" mesh model are larger than those from the "very coarse" and "coarse" mesh models. At the same time, with

Table 1 Mesh resolution

Resolution	N_H	N_L	N
Very coarse	3	65	22,800
Coarse	4	81	30,750
Normal	6	109	46,000
Fine	8	130	62,400

the "normal" mesh resolution, the wave heights are almost equal to those obtained from the "fine" resolution model. This indicates that the "normal" mesh resolution is sufficient for wave numerical simulations.

2.2 Model validation

2.2.1 Wave generation and dissipation

A 2D numerical wave flume 60 m long and 2 m high is established using the aforementioned governing equations and boundary conditions. The x direction is the wave propagation direction, and the y direction is the direction of water depth (as shown in Fig. 2). A second-order Stokes wave is generated using the velocity wave generation method on the left side of the numerical flume. A wave dissipation region with width twice the wavelength and height the same as that of the flume is established on the right side of the flume to eliminate wave reflection at the end of the flume. The wave dissipation coefficient varies linearly from 0 at the starting point of the wave dissipation region to 1 at the end of the flume. Figure 2 shows a schematic diagram of the numerical flume model.

Six wave height meters (numbered 1 to 6 from left to right) are set up in the wave and wave dissipation regions in the flume. The #1 wave height meter in the wave region is 10 m from the wave generation board. Four wave height meters (#1, #2, #3 and #4) are spaced at 10 m intervals in the wave region. Two wave height meters (#5 and #6) are set up in the wave dissipation region, 57 and 59.5 m from the wave generation board, respectively. (See Table 2 for details.)

The computational domain is divided into three regions: regions 1, 2 and 3 (as shown in Fig. 3). Among them, region 2 is near the still water surface. The computational domain is discretized by a structured grid (as shown in Fig. 3). To finely capture the location of the free surface, the grid is refined. The grid cells in the refined region are 0.06 m long and 0.02 m wide. Regions 1 and 3 are unrefined regions, in which the grid cells are 0.06 m long and 0.04 m wide. The mesh sizes in the three different regions and the dimensions of these three regions are detailed in Table 3.

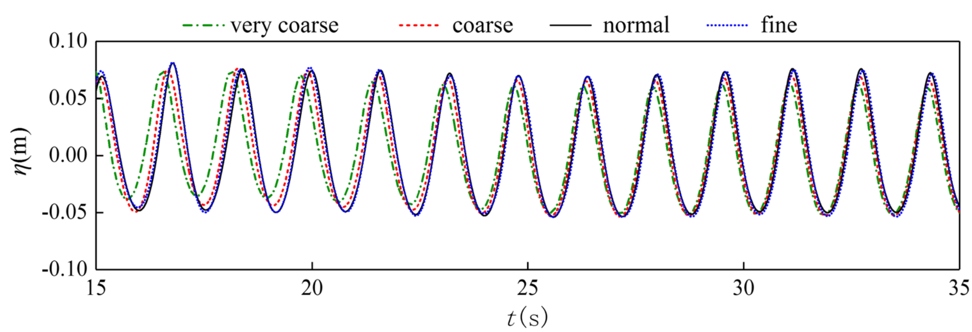

Fig. 1 Time series of surface elevation from numerical models with four mesh resolutions

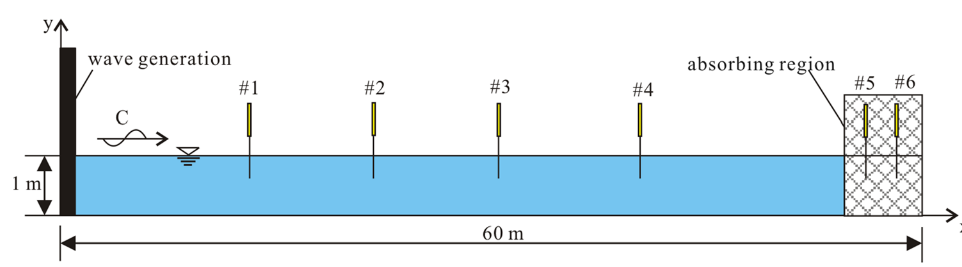

Fig. 2 Sketch of the empty flume

Table 2 Position of wave height meters

Number	#1	#2	#3	#4	#5	#6
Distance from the wave plate (m)	10	20	30	40	57	59.5

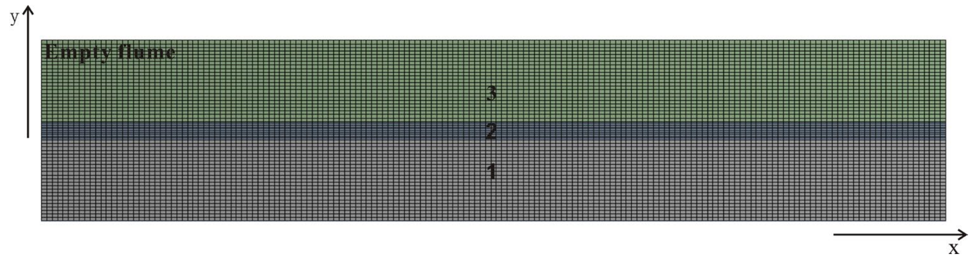

Fig. 3 Sketch of part of the empty flume grid

Table 3 Mesh sizes and dimensions of three regions

Regions	1	2	3	
Dimensions	Length (m)	60	60	60
	Width (m)	0.8	0.4	0.8
Mesh sizes	Length (m)	0.06	0.06	0.06
	Width (m)	0.04	0.02	0.04

This numerical model is used to simulate a second-order Stokes wave ($h=1$ m; $H=10$ cm; $T=1.8$ s). In addition, the wave surface elevation at the locations $x=10$, 20, 30, 40, 57 and 59.5 m away from the wave generation paddle is compared with the theoretical values for second-order Stokes waves (as shown in Fig. 4). The free surface displacement monitored by the #1 to #6 wave height meters at different distances from the wave generation board is in good agreement with the theoretical results of the second-order Stokes wave, demonstrating that the numerical model constructed in this study can generate steady, reliable, regular waves (Fig. 4a–d). A significant decrease in the wave surface elevation can be found at the #5 wave height meter in the wave dissipation region (Fig. 4e). The wave has almost completely dissipated at the #6 wave height meter at the end of the flume (Fig. 4f). This result demonstrates that the wave dissipation region of the numerical model constructed in this study can effectively eliminate the reflected wave on the right side of the flume.

2.2.2 DFPT and DAPT breakwaters

To examine the reliability of the constructed numerical model in the calculation of DFPT open breakwaters, K_t is calculated using the numerical model based on the following relevant parameters used by Guo et al. [19] in their experiment on a DFPT open breakwater: length of each flat

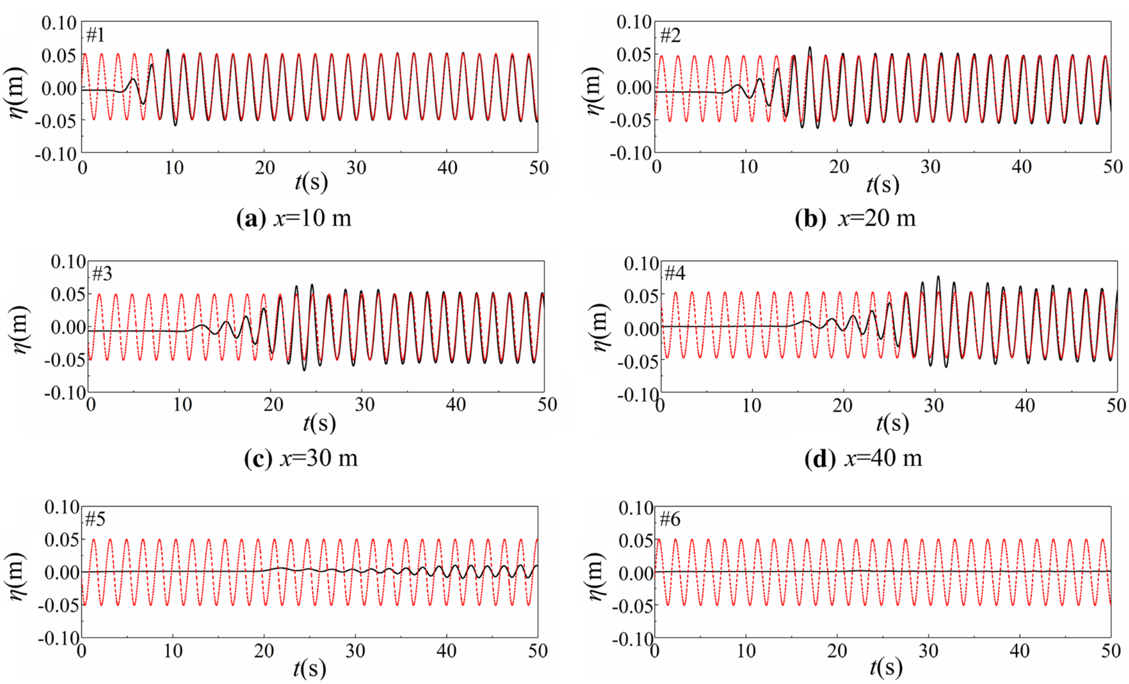

(a) x=10 m (b) x=20 m (c) x=30 m (d) x=40 m (e) x=57 m (f) x=59.5 m

Fig. 4 Comparison between numerical and theoretical results of the wave surface

Table 4 Parameters used in the DFPT experiment

Parameters	Symbols	Units	Ranges
Length of each flat plate	W	m	1
Thickness of each flat plate	d_1	m	0.01
Spacing between two flat plates	S	m	0.10
Water depth	h	m	0.48
Wave period	T	s	1.80
Wave height	H	m	0.06, 0.08, 0.10, 0.12, 0.14

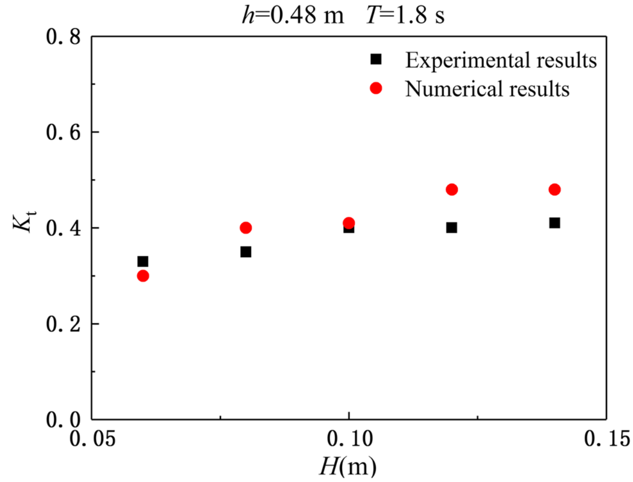

Fig. 6 Comparison between numerical and theoretical results of the transmission coefficients

plate W: 1 m; thickness of each flat plate d1: 0.01 m; spacing between two flat plates S: 0.10 m; h: 0.48 m; T: 1.80 s; and H: 0.06, 0.08, 0.10, 0.12 and 0.14 m. (See Table 4 for details.)

The two-dimensional numerical model was set in the same way as that used by Guo et al. [19], considering the two directions of wave propagation and water depth. Figure 5 shows a schematic diagram of the numerical flume model in the calculation of DFPT breakwaters. The #1 wave height meter is 4.46 m from the back end of the DFPT breakwater. Based on the wave height duration curve measured by the #1 wave gauge, the transmitted wave height H_t is calculated using the upward zero-crossing method. On this basis, K_t is calculated using Eq. (9):

$$K_t = \frac{H_t}{H_i} \tag{9}$$

where H_t is the transmitted wave height and H_i is the incident wave height.

A comparison (Fig. 6) shows that the K_t values obtained using the numerical model constructed in this study are in good agreement with the experimental results obtained by Guo et al. [19], demonstrating that the numerical model constructed in this study can be used to investigate the wave dissipation performance of DFPT open breakwaters.

To examine the reliability of the constructed numerical model in the calculation of APT open breakwaters, an experiment on the wave dissipation performance of the DAPT open breakwater was conducted using the large wave–current flume in the Port and Waterway Laboratory at the School of Civil Engineering of Ludong University. The wave–current experimental flume was 60 m long, 2 m wide and 1.8 m high. An active absorption wave generator capable of generating regular waves with a steady waveform and high repeatability within a period of 0.5–5.0 s was installed at the one end of the flume. The other end of the flume consisted of a gravel wave dissipation section, which dissipated wave energy to reduce wave reflection. We executed some runs with the wave maker and registered the free surface displacement at the wave meters before the experiment, and the wave heights were measured using LG1-60 wave height meters developed and manufactured by Tianjin Port Engineering Institute Co. Ltd. A 36-m-long poly(methyl methacrylate) (PMMA) plate was used to divide the flume along the transverse direction into two small flumes 0.8 and 1.2 m wide.

A DAPT open breakwater model was placed in the 0.8-m-wide small flume. Two wave height meters (#1 and #2) spaced 0.74 m apart were placed in the flume (as shown in Fig. 7). The #2 wave height meter was 4.46 m from the front end of the DAPT open breakwater. The DAPT open breakwater model, made of PMMA, was fixed onto the bottom of the flume using four long stainless steel screws (as shown in Fig. 8).

Fig. 5 Numerical flume sketch of the double flat plate-type breakwater

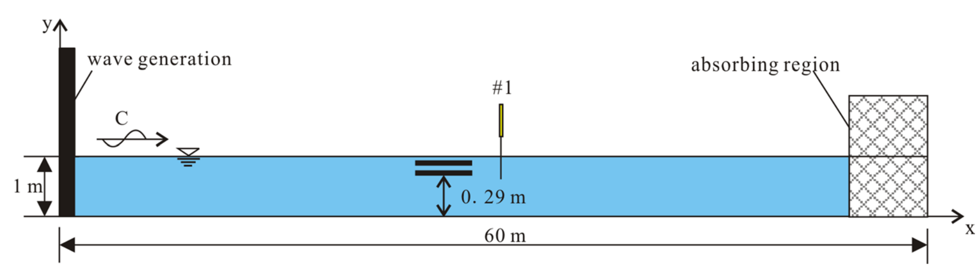

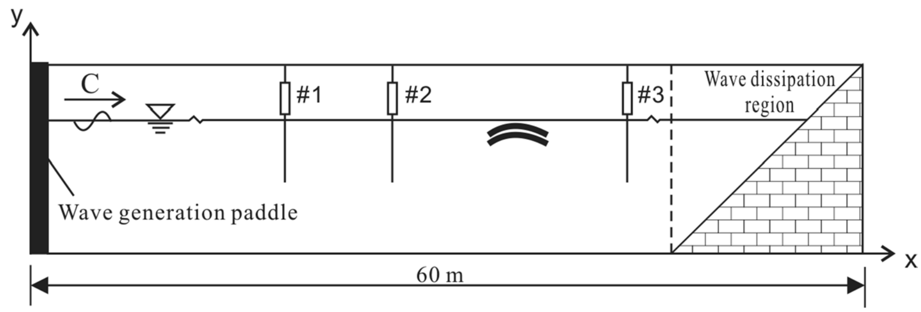

Fig. 7 Diagram of the experimental model of the double-arc-shaped plate-type breakwater

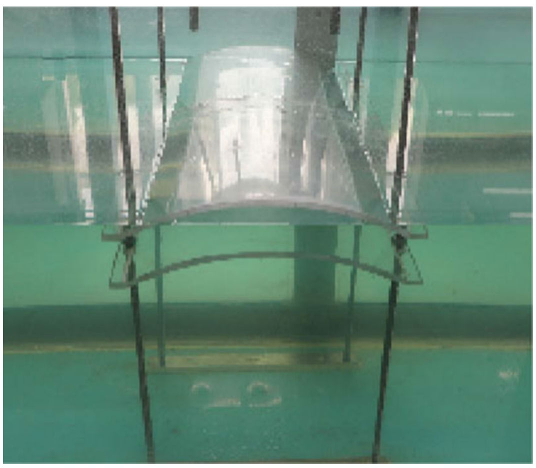

Fig. 8 Image of the double-arc-shaped plate-type breakwater

Table 5 Parameters used in the DAPT experiment

Parameters	Symbols	Units	Ranges
Length of each arc plate	W	m	0.45
Thickness of each arc plate	d_1	m	0.01
Spacing between two arc plates	S	m	0.10
Height of each arc plate	d_0	m	0.10
Water depth	h	m	0.60
Wave period	T	s	1.20, 1.40
Wave height	H	m	0.06

The arc-shaped plate had lengths of 0.45 m on the wave-facing side and 0.79 m on the back-wave side (the dimensions of the arc-shaped plate were designed to facilitate fixation of the model within the flume), a height of 0.10 m and a thickness of 0.01 m, with spacing between two flat plates S: 0.10 m (Table 5).

A numerical model for interactions between waves and the aforementioned DAPT open breakwater was constructed using the previously described numerical method. Wave surface displacement/elevation time histories were calculated at the #1 and #2 wave height meters under two scenarios ($h = 0.60$ m, $T = 1.20$ s and $H = 0.06$ m; $h = 0.60$ m, $T = 1.40$ s and $H = 0.06$ m). The results were compared with the wave surface displacement/elevation time history obtained from the physical model experiment (Fig. 9). When $T = 1.2$ s and 1.4 s, the time was 23.6 s and 22.5 s, corresponding to $t = 0$ in Fig. 9 after the beginning of the wave simulation, respectively. As shown in Fig. 9, the wave surface displacement/elevation time history curves calculated using the constructed numerical model are in relatively good agreement with the wave surface displacement/elevation time history curves obtained from the physical experiment at various test points under various conditions, demonstrating that the constructed numerical model can be used to study the wave dissipation performance of DAPT open breakwaters.

3 Model design and calculation parameters

3.1 Model design

Two open breakwater structures, namely a DFPT breakwater (Fig. 10a) and a DAPT breakwater (Fig. 10b), were designed (plate thickness 0.02 m; plate width 1 m). The arc-shaped plate height (d_0) was used to describe the radius of the arc ($d_0 = 0.1$ m for the DAPT breakwaters; $d_0 = 0$ m for the DFPT breakwater). The two flat plates that constituted the DFPT breakwater and the two arc-shaped plates that constituted the DAPT breakwater each had a spacing of 0.08 m between them. The relative wavelength (λ/W) ranged from 2.60 to 5.58. Table 6 summarizes the parameters in detail.

3.2 Calculation parameters

In the calculation, water depth (h) is set to 1.0 m. The wave period (T) ranges from 1.3 to 2.1 s. Two values of wave height (H) (0.12 and 0.14) and three values of the submerged depth (D) (−0.04, 0 and 0.04 m) are used. If the model scale is 1:30, the corresponding prototype wave periods are 7.12 s, 8.22 s, 9.31 s, 10.41 s and 11.50 s and the wave heights are 3.6 m and 4.2 m. For the DFPT open breakwater, taking the upper plate surface as the reference line, below the water

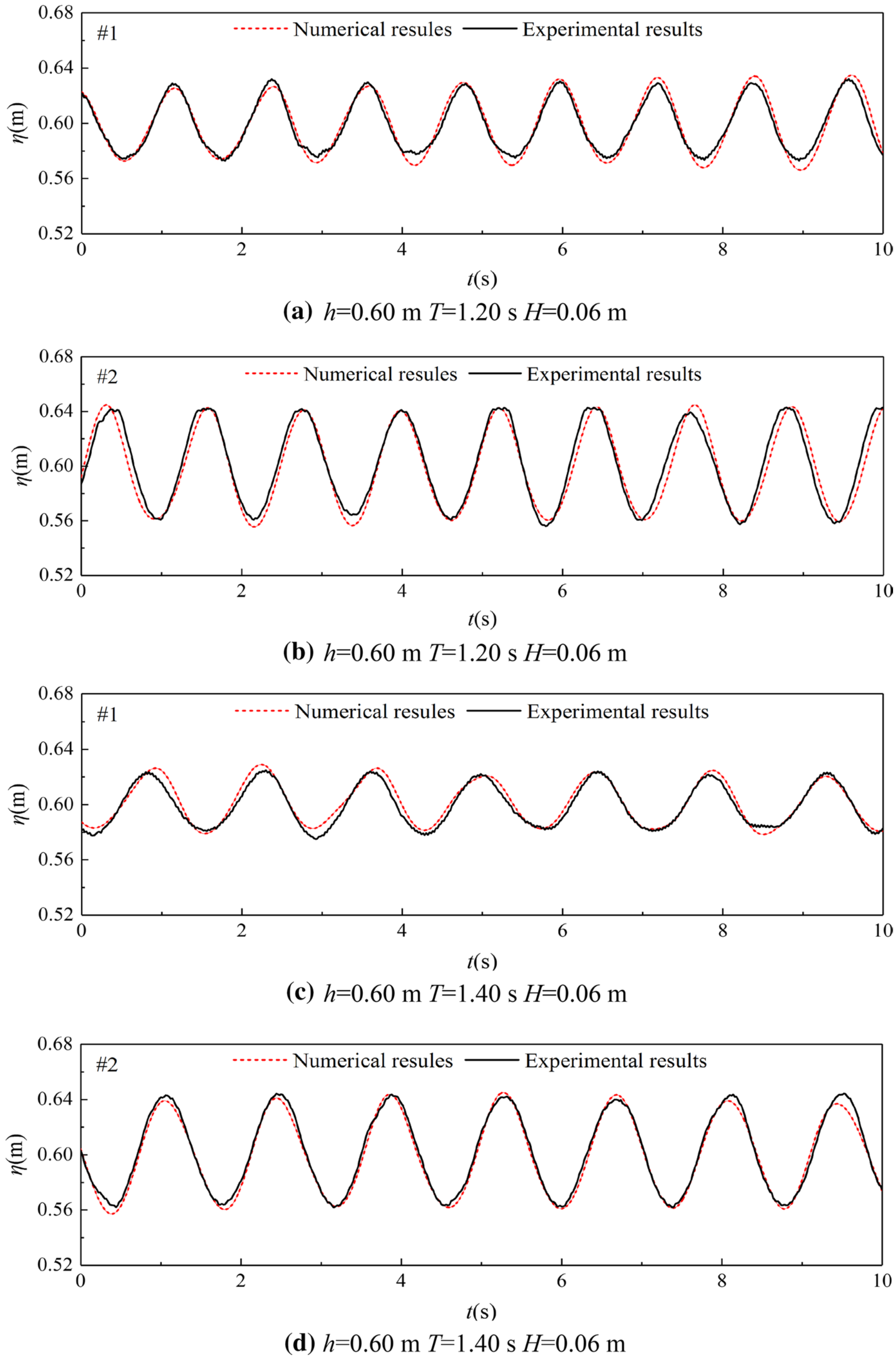

Fig. 9 Comparison between numerical and physical experimental results of the wave surface

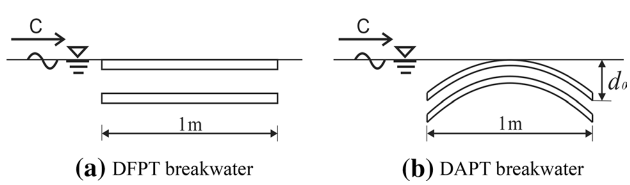

Fig. 10 Sketches of flat and arc-shaped plate-type open breakwaters

surface is positive and above the water surface is negative. For the DAPT open breakwaters, taking the tangent line at the highest point on the upper arc-shaped plate surface as the reference line, below the water surface is positive and above the water surface is negative. Table 7 details the parameter range considered in the numerical simulations.

Based on the characteristics of the two plate-type open breakwater structures, grid generation is performed in the computational domain using various partitioning methods.

Table 6 Model parameters

Model scale	Model parameters	Symbols	Units	Ranges	Real ranges
1:30	Height of plates	d_0	m	0, 0.1	0, 3.0
	Spacing between the plates	S	m	0.08	2.40
	Relative wavelength	λ/W	/	2.60–5.58	2.60–5.58

Table 7 Numerical parameters

Simulation parameters	Symbol	Units	Ranges
Water depth	h	m	1.0
Wave period	T	s	1.3, 1.5, 1.7, 1.9, 2.1
Wave height	H	m	0.12, 0.14
Wavelength	λ	m	2.60, 3.35, 4.11, 4.85, 5.58
Submerged depth	D	m	−0.04, 0, 0.04
Wave steepness	H/λ	/	0.05, 0.04, 0.03, 0.02
Relative water depth	h/λ	/	0.18, 0.21, 0.24, 0.30, 0.38
Relative submergence depth	D/h	/	−0.04, 0, 0.04
Relative wave height	H/D	/	−0.5, −3.5, 0, 0.5, 3.5

For the DFPT and DAPT open breakwaters, the computational domain is divided into 11 subregions. Regions 2, 5, 6, 7 and 10 are refined regions near the still water surface, with grid cells 0.05 m long and 0.02 m high. In the other regions, the grid cells are 0.05 m long and 0.03 m high (as shown in Fig. 11a, b and Tables 8 and 9).

4 Numerical result analysis and discussion

Numerical models for the interactions between waves and the DFPT and DAPT breakwaters are constructed using the aforementioned numerical method. Each numerical flume is 60 m long and 1.5 m high. The numerical flume for the DAPT open breakwater is described here as an example (as shown in Fig. 12). The DAPT open breakwater model is placed in the mid-rear section of the numerical flume, and its front end is 30 m from the wave generation site. On the left side of the numerical flume is a velocity wave generation region, where long-period steady regular waves can be generated. On the right end of the numerical flume is a wave dissipation region with width twice the wavelength.

According to the Goda two-point method's (Goda and Sizuki [32]) requirement for calculating K_r, two wave height meters (#1 and #2) are placed on the wave-facing side of the open breakwater model to monitor the free surface elevation/displacement time history during the calculation process and separate the heights of the incident and reflected waves (H_i and H_r, respectively). A wave height meter (#3) is placed on the back-wave side of the open breakwater model to analyze K_t. Two wave height meters (#1 and #2) spaced 0.74 m apart are placed in the flume. The #2 wave height meter is 4.46 m from the front end of the DAPT breakwater. The #3 wave height meter is 4.46 m from the back end of the DAPT breakwater. The other calculated parameters are as follows. The values for air and water density are 1.29 kg/m^3 and 1000 kg/m^3, respectively. The values for air and water kinematic viscosity are 14.8×10^{-6} m^2/s and 1.01×10^{-6} m^2/s, respectively. The value for air–water surface tension is 72.75×10^{-3} N/m.

Fig. 11 Sketch of part of the open breakwater grids

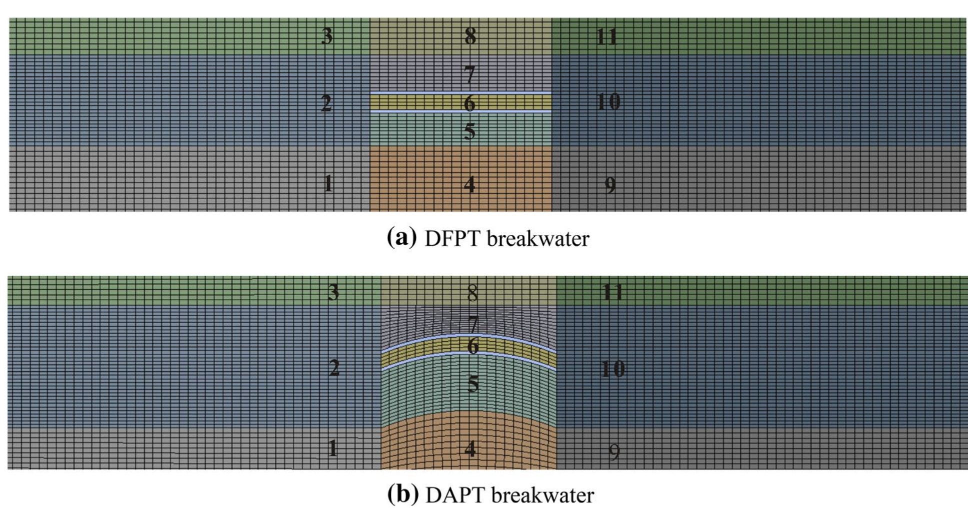

Table 8 Mesh sizes and dimensions of 11 regions for DFPT breakwater

Type	DFPT			
	Dimensions		Mesh sizes	
	Length (m)	Width (m)	Length (m)	Width (m)
1	30	0.75	0.05	0.03
2	30	0.5	0.05	0.02
3	30	0.75	0.05	0.03
4	1	0.75	0.05	0.03
5	1	0.18	0.05	0.02
6	1	0.08	0.05	0.02
7	1	0.2	0.05	0.02
8	1	0.75	0.05	0.03
9	29	0.75	0.05	0.03
10	29	0.5	0.05	0.02
11	29	0.75	0.05	0.03

Table 9 Mesh sizes and dimensions of 11 regions for DAPT breakwater

Type	DAPT			
	Dimensions		Mesh sizes	
	Length (m)	Width (m)	Length (m)	Width (m)
1	30	0.65	0.05	0.03
2	30	0.7	0.05	0.02
3	30	0.65	0.05	0.03
4	1	0.65	0.05	0.03
5	1	0.32	0.05	0.02
6	1	0.08	0.05	0.02
7	1	0.26	0.05	0.02
8	1	0.65	0.05	0.03
9	29	0.65	0.05	0.03
10	29	0.7	0.05	0.02
11	29	0.65	0.05	0.03

4.1 Wave transmission coefficient (K_t)

The K_t of each open breakwater structure was calculated using Eq. (9) mentioned above based on the wave height values monitored using the #3 wave height meter on the back-wave side. Figure 13 shows a comparison of the K_t values for the DFPT and DAPT open breakwaters under the following conditions: h: 1.0 m; H: 0.12 and 0.14 m; and D: −0.04 m, 0 m and 0.04 m. (The tangent line at the highest point on the upper arc-shaped plate surface or the upper flat plate surface is 0.04 m above, at 0.04 m, or 0.04 m below the still water surface, respectively.)

When $D = -0.04$ and 0 m, the K_t of the two open breakwaters increases significantly as λ/W increases (Fig. 13a–d). The K_t value of the DAPT open breakwater is significantly lower than that of the DFPT breakwater (Fig. 13a–d). For the range $2.60 < \lambda/W < 5.58$, the K_t of the DAPT breakwater reaches the lowest value at one extreme of this range for λ/W (Fig. 13a–d). The lowest K_t is 0.19 and 0.15, when $D = -0.04$ m and $H = 0.12$ and 0.14 m, respectively (Fig. 13a, b), and is 0.25 and 0.19 when $D = 0$ m and $H = 0.12$ and 0.14 m, respectively (Fig. 13c, d). When λ/W ranges from 2.60 to 5.58, the K_t of the DAPT open breakwater is up to approximately 45% lower than that of the DFPT open breakwater. Thus, of the two open breakwaters, the transmitted wave of the DAPT open breakwater is lower than that of the DFPT open breakwater.

When $D = 0.04$ m, the K_t of the two open breakwaters increases as λ/W increases (Fig. 13e, f). The K_t of the DFPT open breakwater is significantly lower than that of the DAPT open breakwater (Fig. 13e, f). For the range $2.60 < \lambda/W < 5.58$, the lower value of K_t for the DFPT breakwater is attained at $\lambda/W = 2.60$. When $H = 0.12$ and 0.14 m, the K_t is the lowest (0.25 and 0.28, respectively) (Fig. 13e, f). When λ/W ranges from 2.60 to 5.58, the K_t of the DFPT open breakwater is up to approximately 27% lower than that of the DAPT open breakwater. Thus, of the two open breakwaters, the wave-dissipating performance of the DFPT open breakwater is the most pronounced.

A comprehensive comparison of the K_t values for the two open breakwaters shows a relatively significant difference regarding the transmitted wave between them. When placed at or above the still water surface, the DAPT open breakwater exhibits a lower transmitted wave than that of the DFPT open breakwater. When submerged in the water, the conclusion is the opposite. This phenomenon occurs because when placed at or above the still water surface, the DFPT open breakwater causes waves to undergo shallow-water deformation and breaks by disrupting the

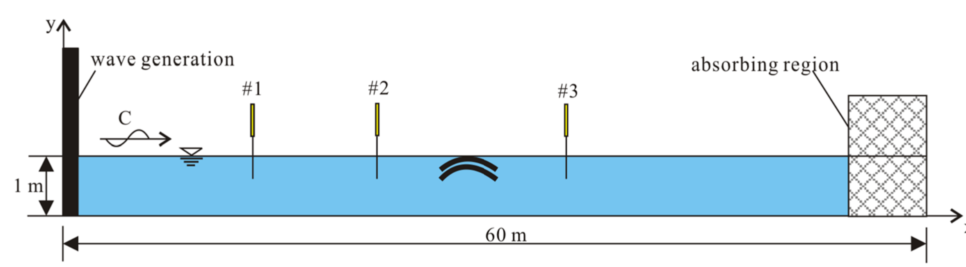

Fig. 12 Numerical flume sketch of the double-arc-shaped plate-type breakwater

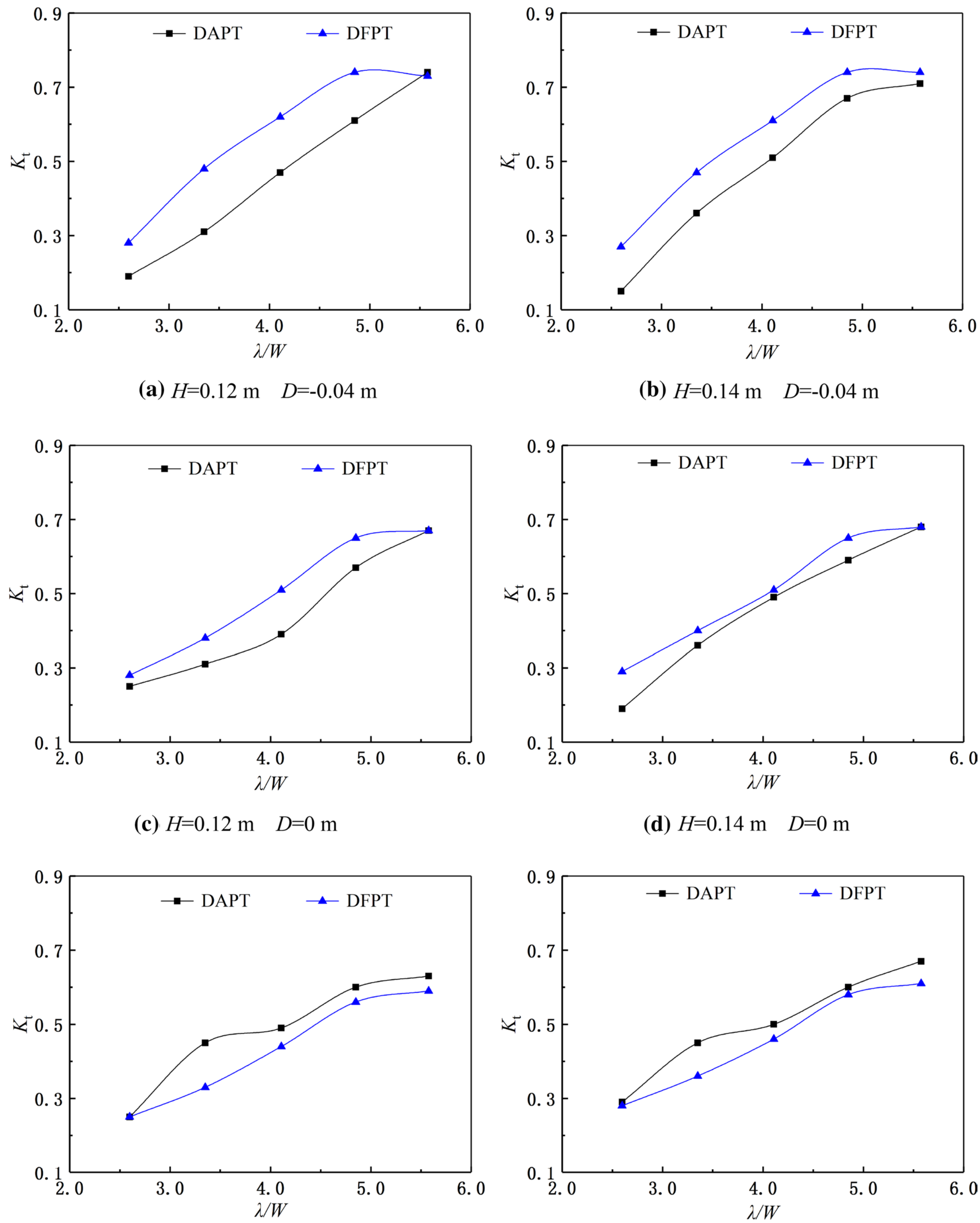

(a) H=0.12 m D=-0.04 m

(b) H=0.14 m D=-0.04 m

(c) H=0.12 m D=0 m

(d) H=0.14 m D=0 m

(e) H=0.12 m D=0.04 m

(f) H=0.14 m D=0.04 m

Fig. 13 Variations in K_t with the relative width for the different plate-type open breakwaters

vertical motion of the water particles, thereby dissipating wave energy. By contrast, the DAPT open breakwater can disrupt both the transverse and vertical motions of water particles, resulting in a shallow-water effect on the waves, which in turn results in more intense wave breaking and more significant wave energy dissipation. The waves may also climb along the breakwater surface, which obstructs the waves to some extent.

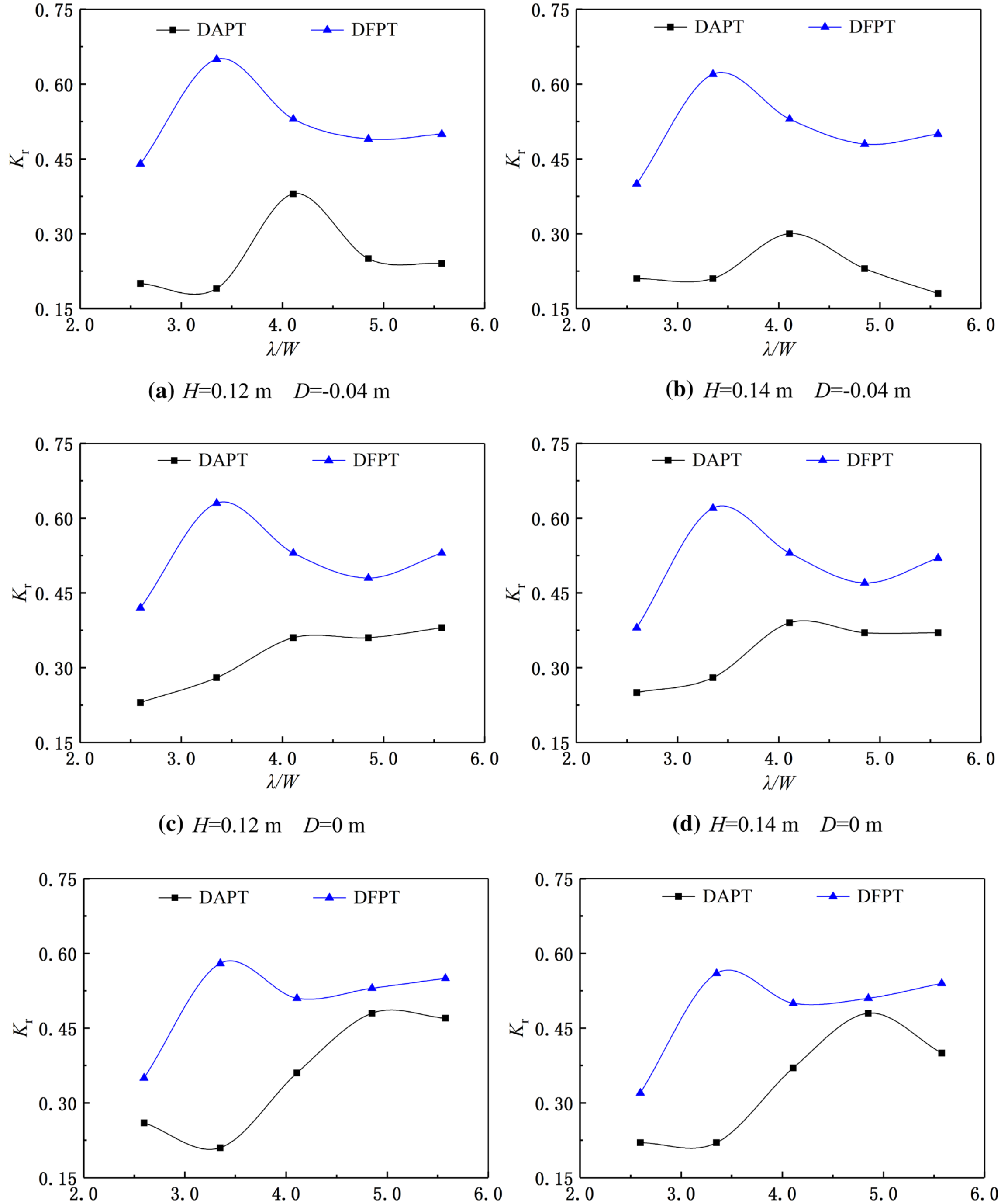

(a) *H*=0.12 m *D*=-0.04 m (b) *H*=0.14 m *D*=-0.04 m

(c) *H*=0.12 m *D*=0 m (d) *H*=0.14 m *D*=0 m

(e) *H*=0.12 m *D*=0.04 m (f) *H*=0.14 m *D*=0.04 m

Fig. 14 Variations in K_r with the relative width for the different plate-type open breakwaters

4.2 Wave reflection coefficient (K_r)

The amplitude of the incident (H_i) and reflected (H_r) waves was separated based on the free surface displacement time history monitored by the #1 and #2 wave height meters using the Goda two-point method (Goda and Suzuki [32]). The K_r of each plate-type open breakwater was calculated by dividing H_r by H_i. Figure 14 shows a comparison of the K_r values for the DFPT and DAPT open breakwaters when $h = 1.0$ m, $H = 0.12$ and 0.14 m, and $D = -0.04$, 0 and 0.04 m.

Under various *D* and *H* conditions, the K_r of the DAPT breakwater first decreases, then increases, and then decreases again as λ/W increases (Fig. 14a–f). For the range $2.60 < \lambda/W < 5.58$, when $D = -0.04$ and 0 m, changes in the trend of K_r occur when λ/W is near 3.35 and 4.11. When $D = 0.04$ m, changes in the trend of K_r occur when λ/W is near 3.35 and 4.85. The K_r of the DFPT breakwater first increases, then decreases, and then increases again as λ/W increases (Fig. 14a–f). When $D = -0.04$ and 0 m, changes in the trend of K_r occur when λ/W is near 3.35 and 4.85. When $D = 0.04$ m, changes in the trend of K_r occur when λ/W is near 3.35 and 4.11. In summary, the K_r of each plate-type open breakwater changes nonmonotonically as λ/W increases. Understanding the changes in K_r with λ/W is of great practical significance to providing guidance for engineering construction.

Of the two open breakwaters, the K_r value of the DAPT open breakwater is significantly lower than that of the DFPT open breakwater. For the range $2.60 < \lambda/W < 5.58$, when $D = -0.04$ m and $H = 0.12$ and 0.14 m, the DAPT open breakwater has lower K_r values of 0.19 and 0.18, respectively, which occur when $\lambda/W = 3.35$ and 5.58, respectively (Fig. 14a, b). When $D = 0$ m and $H = 0.12$ and 0.14 m, the DAPT open breakwater has lower K_r values of 0.23 and 0.25, respectively, which occur when $2.60 < \lambda/W < 5.58$ (Fig. 14c, d). When $D = 0.04$ m and $H = 0.12$ and 0.14 m, the DAPT open breakwater has lower K_r values of 0.21 and 0.22, respectively, which occur when $\lambda/W = 3.35$ (Fig. 14e, f). When λ/W ranges from 2.60 to 5.58, the K_r of the DAPT open breakwater is up to approximately 70% lower than that of the DFPT open breakwater.

4.3 Energy dissipation coefficient (K_d)

The K_d of each plate-type open breakwater was calculated based on the aforementioned results for K_t and K_r using Eq. (10). Figure 15 shows a comparison of the K_d values for the DFPT and DAPT open breakwaters when $h = 1.0$ m, $H = 0.12$ and 0.14 m, and $D = -0.04$, 0 and 0.04 m.

$$K_d^2 = 1 - K_r^2 - K_t^2 \tag{10}$$

Under various D and H conditions, the K_d of the two open breakwaters increases as λ/W increases (Fig. 15a–f). Under approximately 93% of the conditions, the K_d of the DAPT open breakwater is higher than that of the DFPT open breakwater (Fig. 15a–f). When λ/W ranges from 2.60 to 5.58, the K_d of the DAPT open breakwater is up to approximately 1.5-fold higher than that of the DFPT open breakwater.

4.4 Wave energy

When an incident wave interacts with each plate-type open breakwater, the wave energy is transmitted, reflected and dissipated. Figure 16 shows the proportions of the wave energy transmitted, reflected and dissipated by the DAPT and DFPT open breakwaters for different λ/W. The proportions of transmitted, reflected and dissipated wave energy are denoted by TE, RE and DE, respectively, in Fig. 16.

Under the wave parameters used in this study and various submergence conditions, when an incident wave interacts with the DAPT open breakwater, DE decreases with increasing wave period and reaches a higher value at $\lambda/W = 2.60$, accounting for 87–94%, and a smaller value at $\lambda/W = 5.58$, accounting for 38–47% (Fig. 16a–f). TE increases with increasing wave period and reaches a smaller value at $\lambda/W = 2.60$ accounting for 2–8%, and a higher value at $\lambda/W = 5.58$, accounting for 40–55% (Fig. 16a–f). When $D = -0.04$, RE increases first and then decreases with increasing wave period, and the turning point occurs at $\lambda/W = 4.11$, accounting for 14% (Fig. 16a, b). When $D = 0.04$ and 0, RE increases with increasing wave period and reaches a smaller value at $\lambda/W = 2.60$, accounting for 5–7%, and a higher value at $\lambda/W = 5.58$, accounting for 14–22% (Fig. 16c–f).

For $\lambda/W = 2.60$, 3.35, 4.11 and 4.85, most of the energy is dissipated (approximately 94% of the total energy), and the remaining energy is transmitted and reflected (approximately 55% and 3% of the total energy, respectively). For $\lambda/W = 5.58$, most of the energy is transmitted (approximately 55% of the total energy), and the remaining energy is dissipated and reflected (approximately 42% and 3% of the total energy, respectively) (Fig. 16a–f).

When an incident wave interacts with the DFPT open breakwater, DE decreases with increasing wave period and reaches a higher value at $\lambda/W = 2.60$, accounting for 73–82%, and a smaller value at $\lambda/W = 5.58$, accounting for 20–35% (Fig. 16a–f). When $D = -0.04$, TE increases first and then decreases with increasing wave period, and the turning point occurs at $\lambda/W = 4.85$, accounting for 53–55% (Fig. 16a, b). When $D = 0.04$ and 0, TE increases with increasing wave period and reaches a smaller value at $\lambda/W = 2.60$, accounting for 6–8%, and a higher value at $\lambda/W = 5.58$, accounting for 35–46% (Fig. 16c–f). RE increases first and then decreases with increasing wave period, and the turning point occurs at $\lambda/W = 3.35$, accounting for 31–42% (Fig. 16a–f).

When $D = -0.04$, for $\lambda/W = 2.60$, most of the energy is dissipated (approximately 77% of the total energy), and the remaining energy is transmitted and reflected (approximately 7–8% and 16–19% of the total energy, respectively). For $\lambda/W = 3.35$, most of the energy is dissipated and reflected (both approximately 35–42% of the total energy), and the remaining energy is transmitted (approximately 22–23%). For $\lambda/W = 4.11$, DE, RE and TE are approximately the same (all approximately 28–38% of the total energy). For $\lambda/W = 4.85$ and 5.58, most of the energy is transmitted (approximately 53–55% of the total energy), and the

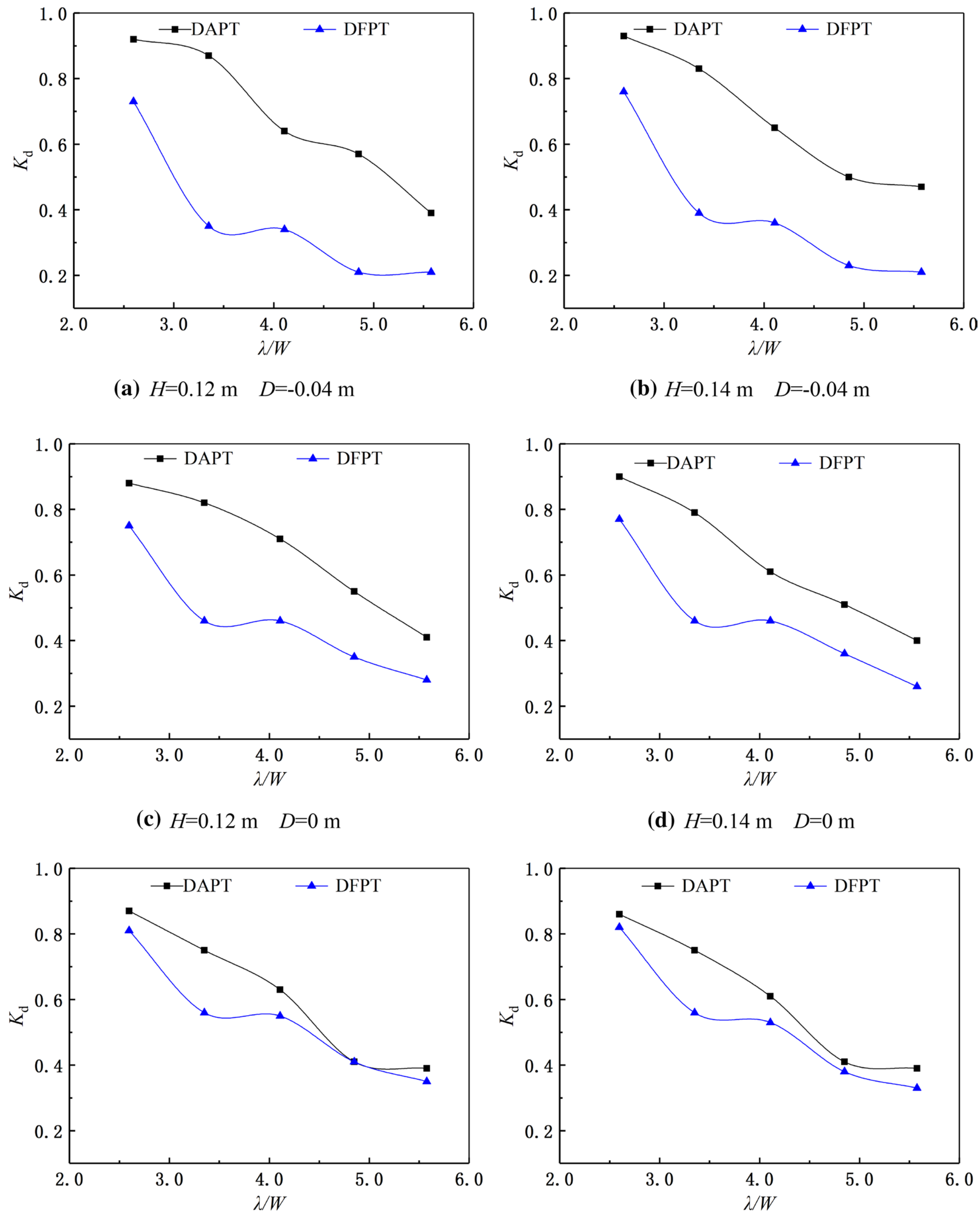

(a) H=0.12 m D=-0.04 m

(b) H=0.14 m D=-0.04 m

(c) H=0.12 m D=0 m

(d) H=0.14 m D=0 m

(e) H=0.12 m D=0.04 m

(f) H=0.14 m D=0.04 m

Fig. 15 Variations in K_d with the relative width for the different plate-type open breakwaters

remaining energy is dissipated and reflected (both approximately 20–25% of the total energy) (Fig. 16a, b). When $D=0$, for $\lambda/W=2.60$ and 3.35, most of the energy is dissipated (approximately 46–78% of the total energy), and the remaining energy is transmitted and reflected (approximately 8–16% and 14–40% of the total energy, respectively). For $\lambda/W=4.11$, most of the energy is dissipated (approximately 46% of the total energy), and the remaining energy is transmitted and reflected (both approximately 26–28% of the total energy). For $\lambda/W=4.85$ and 5.58, most of the energy

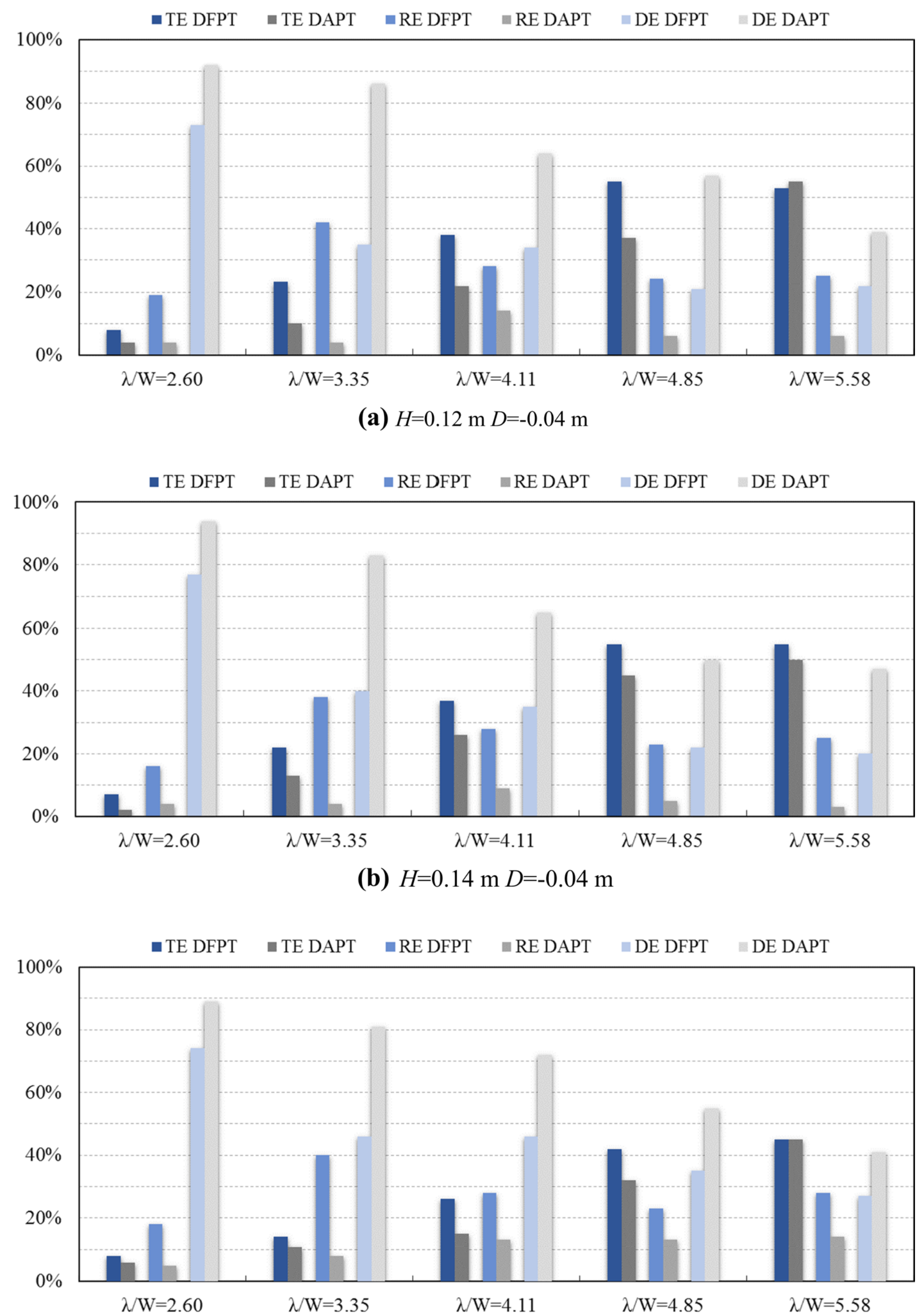

(a) *H*=0.12 m *D*=-0.04 m

(b) *H*=0.14 m *D*=-0.04 m

(c) *H*=0.12 m *D*=0 m

Fig. 16 Wave energy conversion proportions of the two breakwaters for different λ/W

is transmitted (approximately 42–46% of the total energy), and the remaining energy is dissipated and reflected (approximately 27–36% and 22–28% of the total energy, respectively) (Fig. 16c, d). When $D=0.04$, for $\lambda/W=2.60$, 3.35 and 4.11, most of the energy is dissipated (approximately 54–82% of the total energy), and the remaining energy is transmitted and reflected (approximately 6–21% and 10–34% of the total energy, respectively). For $\lambda/W=4.85$ and 5.58, the wave energy is uniformly dissipated, transmitted and reflected (Fig. 16e, f).

Under the same submergence condition, significant differences in the wave energy conversion between the different plate-type open breakwaters are observed. DE of the DAPT breakwater is higher than that of the DFPT breakwater, and the maximum increase is 1.71 times at $D=0.04$, $H=0.14$ and $\lambda/W=4.85$ (Fig. 16a–f). RE of the DAPT breakwater is smaller than that of the DFPT breakwater. The minimum percentage reduction is 12% at $D=0.04$, $H=0.14$ and $\lambda/W=4.85$, and the maximum percentage reduction is 90% at $D=-0.04$, $H=0.12$ and $\lambda/W=3.35$ (Fig. 16a–f). When $D=-0.04$ and 0, TE of the DAPT breakwater is smaller than that of the DFPT breakwater,

Fig. 16 (continued)

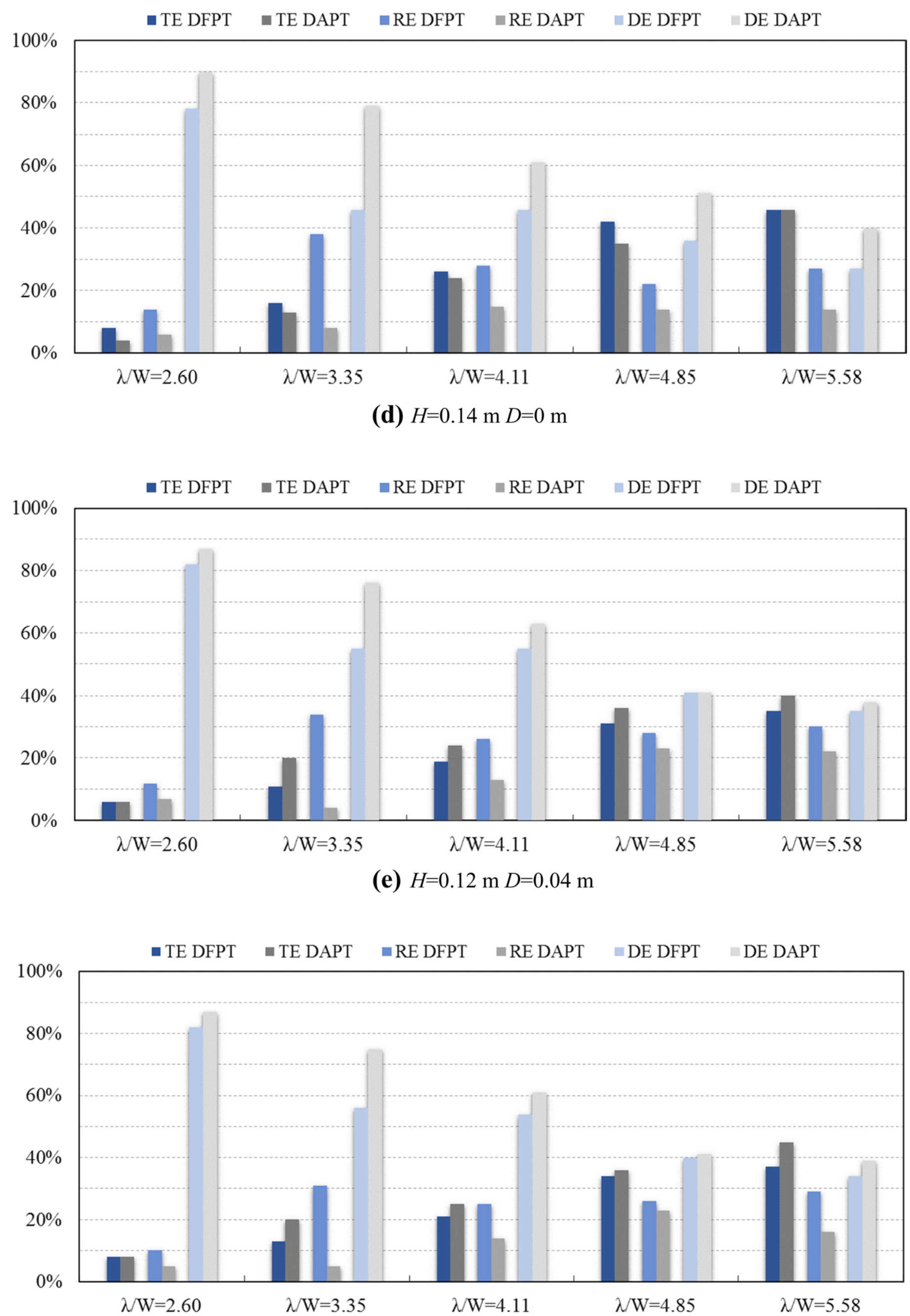

(d) H=0.14 m D=0 m

(e) H=0.12 m D=0.04 m

(f) H=0.14 m D=0.04 m

and the maximum percentage reduction is 71% at $D=-0.04$, $H=0.14$ and $\lambda/W=2.60$ (Fig. 16a–d). When $D=0.04$, TE of the DAPT breakwater is larger than that of the DFPT breakwater, and the minimum increase is 82% at $D=0.04$, $H=0.12$ and $\lambda/W=3.35$ (Fig. 16e, f).

5 Conclusions

In this study, the DAPT breakwater with higher wave dissipation performance when placed at or above the still water surface was proposed. The numerical models of the interactions between waves and various plate-type open breakwaters were constructed using the Navier–Stokes equations, and their correctness was validated. Based on these models, the wave dissipation performance of the DAPT and DFPT open breakwaters was compared. The following conclusions were obtained under the calculation parameter ranges set in this study:

1. The K_t of the two open breakwaters increases as λ/W increases. When $D = -0.04$ and 0 m, under 90% of the conditions, the DAPT open breakwater has a lower K_t than the DFPT open breakwaters. When $D = 0.04$ m, the DFPT open breakwater has a lower K_t than the DAPT open breakwaters.
2. The K_r of the DAPT open breakwater first decreases, then increases, and then decreases again as λ/W increases. The K_r values of the DAPT open breakwaters are significantly lower than those of the DFPT open breakwater.
3. The K_d of the two open breakwaters increases as λ/W increases. Under approximately 93% of the conditions, the DAPT open breakwater has the highest K_d, followed by the DFPT open breakwaters.
4. When an incident wave interacts with the DAPT open breakwater, most of the energy is dissipated. When an incident wave interacts with the DFPT open breakwater, most of the energy is reflected. No significant differences in the proportions of the wave energy transmitted, reflected and dissipated by the same open breakwater under various D conditions are found. However, significant differences in the wave energy conversion between the two plate open breakwaters considered in this work are observed.
5. By comprehensively considering the four metrics (K_t, K_r, K_d and wave energy conversion) for the two types of open breakwaters, when placed at or above the still water surface, the DAPT open breakwater is found to exhibit higher wave dissipation performance than the DFPT open-type breakwater. In engineering practice, DAPT open breakwaters submerged at suitable depths can be selected based on the specific water conditions.

Acknowledgements The work was jointly supported by the National Science Foundation of China-Shandong United fund (Grant nos. U1706220, U1806227, U1906231), the National Natural Science Foundation of China (Grant nos. 51709140, 51879019, 41471005), the National Key Research Project (2017YFC0505902, 2018YFB1501901) and the Key Laboratory of Coastal Disasters and Defence of the Ministry of Education (Grant no. 201703).

Authors' contributions XL contributed to conceptualization, methodology, and writing—original draft preparation. TX contributed to software, visualization and investigation. QW helped in conceptualization, methodology and presentation of the published work. ZZ visualized and investigated the study. CH supervised the study. WG and XW visualized the study. XX performed writing—reviewing and editing.

Funding The study was funded by the National Science Foundation of China-Shandong United fund (Grant nos. U1706220, U1806227, U1906231), the National Natural Science Foundation of China (Grant nos. 51709140, 51879019, 41471005), the National Key Research Project (2017YFC0505902, 2018YFB1501901) and the Key Laboratory of Coastal Disasters and Defence of Ministry of Education (Grant no. 201703).

Availability of data and material None.

Compliance with ethical standards

Conflict of interest The authors declare that they have no known competing financial interests or personal relationship that could have appeared to influence the work reported in this paper.

References

1. Ursell F (1947) The effect of a fixed vertical barrier on surface waves in deep water. Math Proc Camb Philos Soc 43(3):374–382
2. Koley S, Kaligatla RB, Sahoo T (2015) Oblique wave scattering by a vertical flexible porous plate. Stud Appl Math 135(1):1–34
3. Somervell LT, Santosh G, Thampi AG, Shashikala AP (2018) Estimation of friction coefficient for double walled permeable vertical breakwater. Ocean Eng 156:25–37
4. Hsu HH, Wu YC (1998) Scattering of water wave by a submerged horizontal plate and a submerged permeable breakwater. Ocean Eng 26(4):325–341
5. Liu Y, Li YC, Teng B (2007) Wave interaction with a perforated wall breakwater with a horizontal porous plate. Ocean Eng 34(17–18):2364–2373
6. Liu Y, Li HJ, Li YC (2012) A new analytical solution for wave scattering by a submerged horizontal porous plate with finite thickness. Ocean Eng 42:83–92
7. Rao S, Shirlal KG, Varghese RV, Govindaraja KR (2009) Physical model studies on wave transmission of a submerged inclined plate breakwater. Ocean Eng 36(15–16):1199–1207
8. Liu Y, Li YC (2011) An alternative analytical solution for water-wave motion over a submerged horizontal porous plate. J Eng Math 69(4):385–400
9. Cho IH, Kim MH (2013) Transmission of oblique incident waves by a submerged horizontal porous plate. Ocean Eng 61:56–65
10. Wu JP, Xu L, Mei TL, Yi S, Wang LQ (2014) Numerical simulation of the interaction between surface waves and horizontal plates at free surface. Appl Mech Mater 441:456–460
11. Metallinos AS, Repousis EG, Memos CD (2016) Wave propagation over a submerged porous breakwater with steep slopes. Ocean Eng 111(1):424–438
12. Neelamani S, Rajendran R (2002) Wave interaction with ⊥-type breakwaters. Ocean Eng 29(5):561–589
13. Neelamani S, Rajendran R (2002) Wave interaction with T-type breakwaters. Ocean Eng 29(2):151–175
14. Neelamani S, Gayathri T (2006) Wave interaction with twin plate wave barrier. Ocean Eng 33(3):495–516
15. Zhan JM, Chen XB, Gong YJ, Hu WQ (2017) Numerical investigation of the interaction between an inverse T-type fixed/floating breakwater and regular/irregular waves. Ocean Eng 137(1):110–119
16. Usha R, Gayathri T (2005) Wave motion over a twin-plate breakwater. Ocean Eng 32(8–9):1054–1072
17. Wang Y, Wang G, Li G (2006) Experimental study on the performance of the multiple-layer breakwater. Ocean Eng 33(13):1829–1839

18. Li JB, Zhang NC, Guo CS (2010) Numerical simulation of waves interaction with a submerged horizontal twin-plate breakwater. China Ocean Eng 24(4):627–640
19. Guo CS, Zhang NC, Li YY (2011) Experimental study on the performance of twin plate breakwater. China Ocean Eng 25(4):650–652
20. Cho IH, Koh HJ, Kim JR, Kim MH (2013) Wave scattering by dual submerged horizontal porous plates. Ocean Eng 73:149–158
21. Zhang ZQ, Luan MT, Wang K (2013) Flow field analysis of submerged horizontal plate type breakwater. China Ocean Eng 27(6):821–828
22. Liu Y, Li HJ (2014) Wave scattering by dual submerged horizontal porous plates: further results. Ocean Eng 81:158–163
23. Fang ZC, Xiao LF, Kou YF, Li J (2018) Experimental study of the wave-dissipating performance of a four-layer horizontal porous-plate breakwater. Ocean Eng 151:222–233
24. Wang K, Shi PF, Ghen YC, Bian J, Xin H, Cheng XM (2016) Study on hydrodynamic characteristics of submerged upper arc-shaped plate type breakwater. J Ship Mech 20(5):549–557
25. Li XY, Wang Q, You ZJ, Guo WJ, Zhang JB, Zhan C, Zhang ZC, Wang LX, Li Q (2020) Wave attenuation performance and the influencing factors of a lower arc-plate breakwater. J China Ocean Eng 34(1):1–10
26. Wang GY, Ren B, Wang YX (2016) Experimental study on hydrodynamic performance of arc plate breakwater. Ocean Eng 111:593–601
27. Li XY, Ren B, Wang GY, Wang YX (2011) Numerical simulation of hydrodynamic characteristics on an arc crown wall using volume of fluid method based on BFC. J Hydrodyn 23(6):767–776
28. Vermeire BC, Witherden FD, Vincent PE (2017) On the utility of GPU accelerated high-order methods for unsteady flow simulations: a comparison with industry-standard tools. J Comput Phys 334:497–521
29. Higuera P, Losada IJ, Lara JL (2015) Three-dimensional numerical wave generation with moving boundaries. Coast Eng 101:35–47
30. Deng SY (2015) Current situation and prospects of development for numerical wave technology. Wave Conserv Sci Technol Econ 21(4):5–7
31. Zheng YN, Liu Z, Chen CP, Zhan JX (2015) Study on the two-dimension numerical wave tank based on fluent. China Offshore Platform 30(6):60–70
32. Goda Y, Suzuki Y (1976) Estimation of incident and reflected waves in random wave experiments. In: Proceedings of the 10th coastal engineering conference, vol 1. ASCE, New York, pp 828–845